

# Site-Specific Spin Reorientation in Antiferromagnetic State of Quantum System $\text{SeCuO}_3$

Nikolina Novosel,<sup>1</sup> William Lafargue-Dit-Hauret,<sup>2</sup> Željko Rapljenović,<sup>1</sup> Martina Dragičević,<sup>1</sup>  
Helmuth Berger,<sup>3</sup> Dominik Cinčić,<sup>4</sup> Xavier Rocquefelte,<sup>2,\*</sup> and Mirta Herak<sup>1,†</sup>

<sup>1</sup>*Institute of Physics, Bijenička c. 46, HR-10000 Zagreb, Croatia*

<sup>2</sup>*Institut des Sciences Chimiques de Rennes UMR 6226,*

*Université de Rennes 1, Campus de Beaulieu, 35042 Rennes, France*

<sup>3</sup>*Institut de Physique de la Matière Complexe, EPFL, CH-1015 Lausanne, Switzerland*

<sup>4</sup>*Department of Chemistry, Faculty of Science, University of Zagreb, Horvatovac 102A, HR-10000 Zagreb, Croatia*

(Dated: July 21, 2022)

We report on the magnetocrystalline anisotropy energy (MAE) and spin reorientation in antiferromagnetic state of spin  $S = 1/2$  tetramer system  $\text{SeCuO}_3$  observed in torque magnetometry measurements in magnetic fields  $H < 5$  T and simulated using density functional calculations. We employ simple phenomenological model of spin reorientation in finite magnetic field to describe our experimental torque data. Our results strongly support collinear model for magnetic structure in zero field with possibility of only very weak canting. Torque measurements also indicate that, contrary to what is expected for uniaxial antiferromagnet, in  $\text{SeCuO}_3$  only part of the spins exhibit spin flop instead all of them, allowing us to conclude that AFM state of  $\text{SeCuO}_3$  is unconventional and comprised of two decoupled subsystems. Taking into account previously proposed site-selective correlations and dimer singlet state formation in this system, our results offer further proof that AFM state in  $\text{SeCuO}_3$  is composed of a subsystem of AFM dimers forming singlets immersed in antiferromagnetically long-range ordered spins, where both states coexist on atomic scale. Furthermore, we show, using an ab-initio approach, that both subsystems contribute differently to the MAE, corroborating the existence of decoupled subnetworks in  $\text{SeCuO}_3$ . Combination of torque magnetometry, phenomenological approach and DFT simulations to magnetic anisotropy presented here represents a unique and original way to study site-specific reorientation phenomena in quantum magnets.

## I. INTRODUCTION

Low-dimensional spin systems represent a fertile ground to study the influence of quantum effects on the formation of exotic states of matter. Zero-dimensional (0D) systems, in particular, are of significance since simple finite lattices represent fruitful playground for theoretical investigations, while, at the same time, 0D magnetic lattices can be found in real materials allowing the test of theory. The simplest example of 0D system is a spin dimer consisting of two spins coupled by exchange energy  $J$ . Two allowed states are singlet and triplet separated by an energy gap  $J$  and the ground state is determined by the sign of  $J$  (antiferromagnetic or ferromagnetic coupling). In real materials small, but finite, interactions between the 0D units can lead to long range magnetic ordering. This, combined with quantum effects of underlying 0D magnetic units, can lead to exotic phase diagrams where different phases can be obtained by tuning the relative strength of the exchange couplings.

Another example of 0D system is a spin tetramer where four spins  $S_a$ ,  $S_b$ ,  $S_c$  and  $S_d$  interact forming a 0D magnetic unit with slightly more complex excitation spectrum than found in spin dimer [1]. When coupling between spins  $S_a$  and  $S_b$  is equal to coupling between spins  $S_c$  and  $S_d$ , spin Hamiltonian of this system can be written as

$$\mathcal{H} = J_{12} (\mathbf{S}_a \cdot \mathbf{S}_b + \mathbf{S}_c \cdot \mathbf{S}_d) + J_{11} (\mathbf{S}_b \cdot \mathbf{S}_c). \quad (1)$$

Interesting limit for spin tetramer is the case when the coupling  $J_{11}$  between the two spins in the middle,  $S_b$  and  $S_c$ , is antiferromagnetic and much stronger than the coupling  $J_{12}$  with two spins on the sides of tetramer,  $S_a$  and  $S_d$  (see Fig. 1). In this case  $S_b$  and  $S_c$  are expected to form a singlet state which persists in the background of weakly connected paramagnetic spins  $S_a$  and  $S_d$ . At low temperatures weak intertetramer interactions can lead to long-range magnetic order. When this happens, the question arises whether singlet states are broken with  $S_b$  and  $S_c$  spins joining the long-range order, or they somehow persist as singlets in the background of long-range magnetically ordered spins  $S_a$  and  $S_d$ . Latter scenario was proposed by Hase *et al.* for spin tetramer system  $\text{CdCu}_2(\text{BO}_3)_2$  based on high field magnetization measurements [2], and it was recently confirmed by nuclear magnetic resonance (NMR) and zero-field muon spin relaxation (ZF- $\mu$ SR) [3]. In the ordered AFM state of  $\text{CdCu}_2(\text{BO}_3)_2$ , spins  $S_a$  and  $S_d$  are related to Cu2 site, while  $S_b$  and  $S_c$  to Cu1 site. In this system, spins of Cu1 atoms form strongly coupled singlets, but at  $T_N = 9.8$  K, antiferromagnetic long-range order sets in due to much weaker intertetramer interactions. Neutron powder diffraction (NPD) measurements on this system reported significant magnetic moment on both Cu1 and Cu2, although smaller on Cu1 [4]. Detailed theoretical investigation of  $\text{CdCu}_2(\text{BO}_3)_2$  showed dominant coupling between Cu1 spins forming AFM dimers, while further couplings forming intratetramer and intertetramer interactions are responsible for low-temperature AFM LRO of spins Cu2 which polarize Cu1 singlet states [5]. Same study revealed that polarization of Cu1 singlets is possible because the field from Cu2 spins is staggered and thus does not commute with the exchange interaction on the dimer [5]. Janson *et al.* further showed that significant magnetic mo-

\* xavier.rocquefelte@univ-rennes1.fr

† mirta@ifs.hr

ment can be induced on Cu1 spins by the staggered field from Cu2 spins [5]. This picture, later confirmed experimentally by NMR and ZF- $\mu$ SR measurements [3], is different from usual long-range order which is induced by interactions between spins. In  $\text{CdCu}_2(\text{BO}_3)_2$  only ordering between Cu2 spins is induced by magnetic interaction, while ordering of Cu1 spins is induced by polarization. The decoupling of Cu1 and Cu2 spins in the ordered state is evidenced by a magnetic anomaly at  $T^* = 6.5$  K observed in NMR which was attributed to reorientation of spins Cu2, while Cu1 remain intact [3]. To better understand how this type of ordering emerges it is important to find and study new systems which might host such exotic behavior.  $\text{SeCuO}_3$  studied in this work is in many aspects similar to  $\text{CdCu}_2(\text{BO}_3)_2$  and thus represents an ideal candidate to study site-selective quantum magnetism, especially since, unlike for the latter, high quality single crystals are available.

Monoclinic  $\text{SeCuO}_3$  was recently proposed to be a host to quantum linear spin tetramer system described by Hamiltonian (1) where site-selective quantum correlations might play a significant role in establishing unusual magnetic properties [6].  $\text{SeCuO}_3$  crystals belong to monoclinic space group  $P2_1/n$  with unit cell parameters  $a = 7.712$  Å,  $b = 8.238$  Å,  $c = 8.498$  Å, and  $\beta = 99.124^\circ$  [7]. Two crystallographically inequivalent copper atoms, Cu1 and Cu2 are present in monoclinic  $\text{SeCuO}_3$ , each surrounded by six oxygen ligands forming Jahn-Teller distorted elongated  $\text{CuO}_6$  octahedra. This ligand configuration suggests  $d_{x^2-y^2}$  orbital state of the unpaired copper spin  $S = 1/2$ . Taking into account local environment of magnetic ion  $\text{Cu}^{2+}$ , it was proposed in Ref. 6 that isolated linear spin tetramers  $\text{Cu}_2\text{-Cu}_1\text{-Cu}_1\text{-Cu}_2$  are present in  $\text{SeCuO}_3$ . Two magnetically inequivalent spin tetramers in  $\text{SeCuO}_3$  are shown in Fig. 1. However, temperature dependence of magnetic susceptibility cannot be explained by the simple tetramer Hamiltonian Eq. (1) [8], even if temperature dependence of  $g$  factor is taken into account [9].

Previous studies of  $\text{SeCuO}_3$  proposed that rotation of macroscopic magnetic axes and temperature dependence of electron  $\mathbf{g}$  tensor in paramagnetic state [6, 9] are not a consequence of temperature change of crystal structure, but rather of a site-selective correlation which emerges from large difference between  $J_{11}$  and  $J_{12}$  couplings [6]. Recent nuclear quadrupole resonance (NQR) study proposed that Cu1 spins are strongly coupled forming a spin singlet state at temperatures  $T < J_{11} \approx 200$  K [10].

Below  $T_N = 8$  K,  $\text{SeCuO}_3$  exhibits long-range antiferromagnetic (AFM) order [6, 9–11]. Temperature dependence of magnetic susceptibility anisotropy in low magnetic field below  $T_N$  is typical for uniaxial antiferromagnet [6, 9]. Spin-flop transition is observed around  $H_{SF} \approx 1.8$  T at  $T = 2$  K when magnetic field is applied along easy axis [6]. Torque magnetometry reveals unusual weak rotation of magnetic axes with temperature in the  $ac$  plane in AFM state [6, 9], while NMR measurements evidence possible rotation of magnetic moments in the AFM state [11] connected to different moments developed on Cu1 and Cu2 spins and different coupling between them. High-field magnetization measurements showed existence of half-step magnetization plateau [11] similar to what was found in previously mentioned  $\text{CdCu}_2(\text{BO}_3)_2$

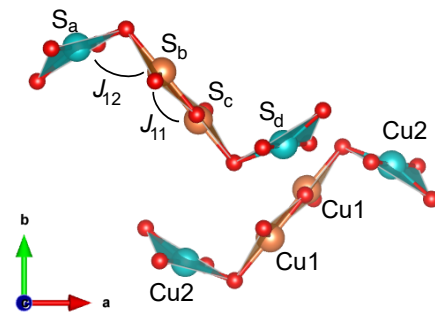


FIG. 1. Two magnetically inequivalent tetramers in  $\text{SeCuO}_3$  as proposed in Ref. 6. Cu1 atoms are orange, Cu2 are blue and O atoms are red. Se atoms are not shown for simplicity.

compound where the plateau emerges from polarization of weakly coupled Cu2 spins while Cu1 dimers remain in singlet state [2].  $^{77}\text{Se}$  NMR measurements revealed different temperature dependence of Cu1 and Cu2 spin-spin relaxation rate  $1/T_2$  in AFM state which could be a signature of a presence of two subsystems in  $\text{SeCuO}_3$ , strongly coupled Cu1 dimers and weakly coupled Cu2 spins [11]. All these observations confirm that  $\text{SeCuO}_3$  represents an ideal new host to study exotic magnetic behavior influenced by quantum phenomena.

Magnetic structure of  $\text{SeCuO}_3$  recently proposed from neutron powder diffraction measurements is highly non-collinear with different magnetic moment values at Cu1 and Cu2 sites,  $m_{\text{Cu1}} \approx 0.4\mu_B$  and  $m_{\text{Cu2}} \approx 0.7\mu_B$  at 1.5 K [10]. NQR measurements obtained slightly smaller value,  $m_{\text{Cu1}} = 0.35\mu_B$ , and also different orientation of the Cu1 moment with respect to  $\text{CuO}_4$  plaquette than observed from neutron diffraction experiment [10]. Obviously, AFM state in  $\text{SeCuO}_3$  is more interesting than a simple uniaxial Néel state and calls for further studies. In this work we experimentally probe magnetic anisotropy of AFM state in  $\text{SeCuO}_3$  using torque magnetometry measurements in magnetic fields  $H \lesssim 5$  T significantly higher than the spin flop field  $H_{SF} \approx 1.8$  T. This allows us to determine the magnetocrystalline anisotropy energy (MAE) of  $\text{SeCuO}_3$  as well as to study field-induced spin reorientation. We complete the description of the MAE by a theoretical investigation based on first-principles calculations.

## II. METHODS

### A. Experimental

Single crystals of monoclinic  $\text{SeCuO}_3$  have been grown by a standard chemical vapor phase method, as described in literature [6].

Magnetic torque was measured by home-built torque apparatus based on torsion of thin quartz fibre. Magnetic field was supplied by Cryogenic Consultants 5 T split-coil superconducting magnet with room-temperature bore. Quartz sample holder is placed in separate cryostat which is mounted in the room-temperature bore of the magnet cryostat. Monitor-

ing and control of the sample temperature was performed by Lakeshore 336 temperature controller. For magnetic torque measurements single crystal of mass  $(246 \pm 8) \mu\text{g}$  was used with  $b$  axis parallel to longest crystal axis and two crystal planes  $(101)$  and  $(10\bar{1})$  easily distinguished.

## B. Theory

The present calculations are based on spin-polarized density functional theory as implemented in the Wien2k package[12] using a full potential linear augmented plane wave method. The Perdew-Burke-Ernzerhof approximation (PBE) [13] is considered for the exchange and correlation part. An Hubbard effective term within the Anisimov approach [14] was used to describe more properly Cu 3d orbitals, allowing us to obtain magnetic moments for copper sites close to  $0.73 \mu_B$ . We also checked our calculations considering the on-site PBE0 hybrid functional[15], giving us similar observations. The  $R_{MT}$  Muffin-Tin radii for Se, Cu and O atoms are set to 1.65, 1.96 and 1.49  $a_0$  and the  $RK_{max}$  to 6. The separation between valence and core states was set to -6 Ry, except for the calculations including zinc atoms (set to -8 Ry, with  $R_{MT} = 1.96$  bohr). The Brillouin zone sampling was done using a  $5 \times 4 \times 4$  k-mesh [16].

## III. RESULTS

### A. Experimental Results

For a simple collinear uniaxial antiferromagnet in low magnetic field  $H \ll H_{SF}$ , magnetization is linearly dependent on magnetic field. Consequently (see Appendix), angular dependence of measured component of magnetic torque  $\tau_z$  is then described by expression

$$\tau_z = \tau_0 \sin(2\varphi - 2\varphi_0), \quad (2)$$

where amplitude  $\tau_0$  is given by

$$\tau_0 = \frac{m}{2 M_{mol}} \Delta\chi_{xy} H^2. \quad (3)$$

$m$  is mass of the sample,  $M_{mol}$  is molar mass and  $H$  is magnitude of applied magnetic field.  $\Delta\chi_{xy} = \chi_x - \chi_y$  is magnetic susceptibility anisotropy in the  $xy$  plane in which magnetic field rotates.  $x$  is the direction of maximal, and  $y$  of minimal susceptibility component in the plane of measurement.  $\varphi$  is goniometer angle and  $\varphi_0$  is the angle at which the field is parallel to  $x$ . Eqs. (2) and (3) show that, in case of linear response, magnetic torque is proportional to  $H^2$  and  $\Delta\chi$  and angular dependence of torque is a sine curve with period  $180^\circ$ . Previously published low-field ( $H \lesssim 0.2$  T) torque data [9] in both paramagnetic and antiferromagnetic state are well described by Eqs. (2) and (3).

Magnetic torque was measured in AFM state at  $T = 4.2$  K by rotating magnetic field in three crystal planes:  $ac$  plane, plane spanned by  $b$  and  $[10\bar{1}]^*$  axes and plane spanned by

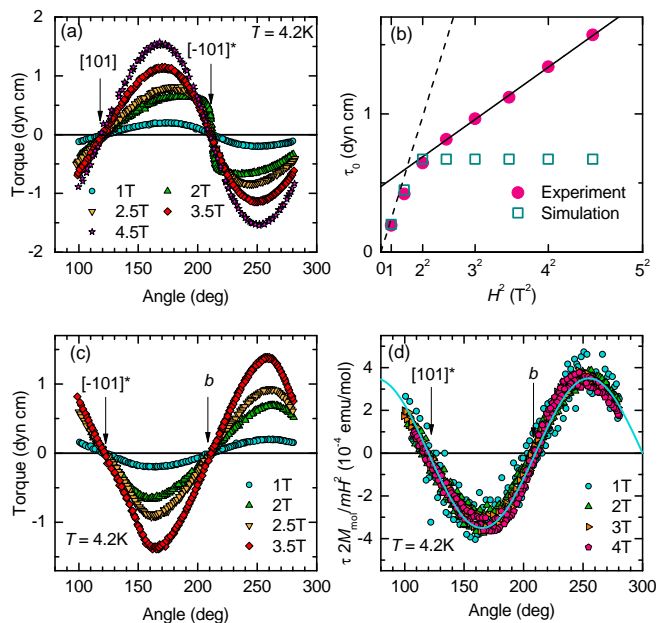


FIG. 2. Angular dependence of torque  $\tau$  measured in three crystal planes in different magnetic fields. (a) Torque measured in the  $ac$  plane. (b) Full symbols: dependence of torque amplitude  $\tau_0$  on  $H^2$  in the  $ac$  plane [see (a)]. Solid line is fit to experimental data for  $H > H_{SF}$ . Dashed line represents expected  $H^2$  dependence of torque amplitude for antiferromagnet with no reorientation (extrapolation of  $H \ll H_{SF}$  data using Eq. (3) and low-field anisotropy data [9]). Empty symbols: result of simulation (see Sec. III B). (c) Angular dependence of torque measured in plane spanned by  $b$  and  $[10\bar{1}]^*$  axes, and (d) plane spanned by  $b$  and  $[101]^*$ . In (d) torque is multiplied by  $2M_{mol}/(mH^2)$  resulting in practically the same curve for all applied fields. This is consistent with no reorientation of spins in this plane [see Eq. (2)]. Angles corresponding to specific crystal directions are pointed by arrows.

$b$  and  $[10\bar{1}]^*$  axes. Angular dependence of torque for these three planes is shown in Fig. 2. With exception of data shown in Fig. 2(d) for plane spanned by  $b$  and  $[10\bar{1}]^*$  axes, measured torque cannot be described by Eq. (2). Torque curves in Figs. 2(a) and 2(c) are not regular sine curves and amplitude of torque does not increase linearly with  $H^2$ , as can be seen for  $ac$  plane in Fig. 2(b). Deviation of torque curves from Eq. (2) is most pronounced in the  $ac$  plane for  $H = 2$  T which is close to the spin flop field  $H_{SF} \approx 1.8$  T, see Fig. 2(a).

For plane spanned by  $b$  and  $[10\bar{1}]^*$  axes we show torque multiplied by  $2M_{mol}/(mH^2)$  in Fig. 2(d). In this way torque measured in different fields gives practically the same curve, which is expected from Eqs. (2) and (3) and implies there is no spin reorientation in this plane. In this work we show that the deviation from low-field behaviour observed in two other crystal planes is a result of the spin axis reorientation induced by magnetic fields comparable to the spin-flop field.

In Fig. 2(b) we plot dependence of torque amplitude  $\tau_0$  on  $H^2$  measured in the  $ac$  plane. Dashed line represents the slope given by  $m/2 M_{mol} \Delta\chi_{xy}$  [see Eq. (3)] with  $\Delta\chi$  obtained from low-field measurements [9]. The deviation from low-

field behavior is observed already for  $H \gtrsim 1.5$  T. Interestingly,  $H^2$  dependence seems to be restored for  $H \geq 2$  T but with much smaller slope which would, according to Eq. (3), correspond to weaker susceptibility anisotropy  $\Delta\chi$ . This result will prove crucial for our interpretation of spin reorientation in  $\text{SeCuO}_3$  and in the following sections we will demonstrate how observed behavior is a direct consequence of site-specific spin reorientation induced by magnetic field comparable to or larger than the spin flop field.

### B. Phenomenological model of spin reorientation in $\text{SeCuO}_3$

Spin reorientation in collinear antiferromagnet in finite applied magnetic field was first proposed by Néel in 1936 [17, 18] who observed that competition between magnetocrystalline anisotropy energy (MAE) and Zeeman energy results in reorientation of spins in such a way to minimize the total energy. MAE determines the spin orientation in zero magnetic field (easy axis direction), while Zeeman energy for antiferromagnet is minimal when the spins are perpendicular to magnetic field. Depending on the magnitude and direction of applied field, spins will be oriented in such a way to minimize the total energy, while still maintaining almost collinear AFM structure due to exchange energy which is much stronger than anisotropy energy. When magnetic field is applied along the easy axis the spins reorient to the direction perpendicular to magnetic field at critical value of magnetic field  $H_{SF}$  called *spin flop* field. Value of spin-flop field depends on magnetocrystalline anisotropy energy, as well as on magnetic susceptibility anisotropy [19]. Spin-flop transition was observed in many antiferromagnets and studied in detail in literature (see e.g. Ref. 20 and references therein). Simple phenomenological approach proposed already by Néel can be used to study field induced spin reorientation in antiferromagnets with different symmetries. Specifically, torque magnetometry measurements can be employed to determine the MAE shape and also to study spin axis reorientation in finite magnetic field. We have successfully used this approach previously to study magnetocrystalline anisotropy in uniaxial antiferromagnet [21], but also in antiferromagnets with higher symmetries and multiple antiferromagnetic domains [22, 23].

In order to employ phenomenological approach in study of macroscopic spin reorientation in collinear antiferromagnets we need to know magnetic susceptibility tensor, as well as magnetocrystalline anisotropy energy (MAE). In accordance with Neumann's principle both susceptibility tensor and MAE of  $\text{SeCuO}_3$  must obey point group symmetry elements of  $P2_1/n$  space group.

Magnetic susceptibility tensor can be determined by torque measurements in low magnetic field, as shown in Appendix. The temperature dependence of magnetic susceptibility anisotropy in AFM state of  $\text{SeCuO}_3$  [6, 9] is typical for uniaxial antiferromagnet: susceptibility goes to zero as temperature decreases from  $T_N$  to zero when magnetic field is applied along easy axis, and is almost temperature-independent along hard and intermediate axes. Our previous torque measurements in low magnetic field [9] have shown that in AFM state

below  $T \approx 6$  K easy magnetic axis is along  $\langle \bar{1}01 \rangle^*$ , while intermediate and hard axes are along  $\langle 101 \rangle$  and  $\langle 010 \rangle = \pm b$  axes, respectively. This allows us to write magnetic susceptibility tensor of AFM state in  $\text{SeCuO}_3$  for  $T \lesssim 6$  K

$$\hat{\chi}_0 = \begin{bmatrix} \chi_{[\bar{1}01]^*} & 0 & 0 \\ 0 & \chi_{[101]} & 0 \\ 0 & 0 & \chi_b \end{bmatrix}. \quad (4)$$

Coordinate system spanned by magnetic eigenaxes in AFM state below  $\approx 6$  K is  $([\bar{1}01]^*, [101], b)$ . This is in accordance with symmetry requirements which dictate that  $b$  axis must be one of magnetic eigenaxes, while two other eigenaxes can have any orientation in the  $ac$  plane [24]. One might note here that measurement of susceptibility tensor allows detection of symmetry breaking which is observed if  $b$  axis no longer represents one of the magnetic eigenaxes, as explained in Appendix. We have performed detailed measurements to determine if there is such symmetry breaking in  $\text{SeCuO}_3$  and, within the small error induced by misorientation of the sample, our results show that symmetry is preserved in AFM state of  $\text{SeCuO}_3$ , in agreement with recent neutron powder diffraction and NQR measurements [10]. Small rotation of magnetic axes observed for  $6 \text{ K} \lesssim T \lesssim T_N = 8 \text{ K}$  [6, 9] is confined to the  $ac$  plane and is thus symmetry-preserving.

Next, we write down the MAE, which also must satisfy point group symmetry operations for  $\text{SeCuO}_3$ , as follows

$$\mathcal{F}_a(\theta, \phi) = K_1 \cos^2 \theta + K_2 \sin^2 \theta \cos 2\phi, \quad (5)$$

where  $\theta$  and  $\phi$  are polar and azimuthal angles in spherical coordinate system, and  $K_1$  and  $K_2$  are anisotropy constants expressed in units of *erg/mol* in this work. In principle, anisotropy energy  $\mathcal{F}_a$  can be written to higher-order terms and can also include extrinsic contributions to anisotropy such as shape anisotropy. However, second order terms, written in Eq. (5), are sufficient to study the reorientation of spin axis in finite magnetic field, as long as we do not try to describe critical behaviour in magnetic field very close to spin flop field [20]. Eq. (5) describes how much energy is needed to rotate the spin axis from the easy axis direction. Depending on the value and sign of anisotropy constants (both can be positive or negative), anisotropy energy (5) can have several different symmetry-allowed shapes. Torque magnetometry is experimental technique which can be employed to experimentally determine actual shape of MAE for specific crystal. As already mentioned, our previous low-field torque results, along with the results shown in Fig. 2 show that easy axis direction in antiferromagnetic phase for  $T \lesssim 6$  K is along the  $\langle \bar{1}01 \rangle^*$  direction. This is, then, the direction of the global minimum of the anisotropy energy (5). Other two extrema then must be along the  $\langle 101 \rangle$  and  $\pm b$  axes directions. Torque results presented in this work find global maximum i.e. hard axis along the  $\pm b$  direction, while intermediate axis is along the  $\langle 101 \rangle$  direction. This puts the following constraints on anisotropy constants:  $K_2 < 0$  and  $K_2 < K_1$ . In Fig. 3 we plot magnetocrystalline anisotropy energy realized in  $\text{SeCuO}_3$ .

In finite magnetic field,  $\mathbf{H}(\psi, \xi)$ , Zeeman energy is given by

$$\mathcal{F}_Z(\psi, \xi) = -\frac{1}{2} \mathbf{H}(\psi, \xi) \cdot \hat{\chi} \cdot \mathbf{H}(\psi, \xi) \quad (6)$$

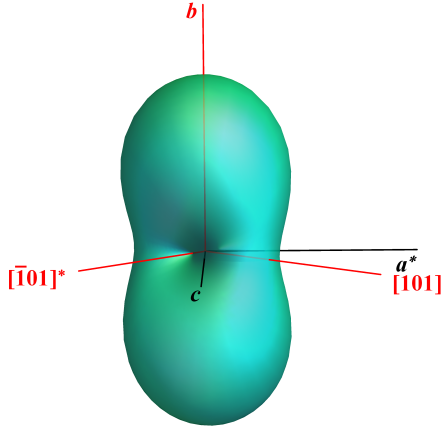


FIG. 3. MAE shape in  $\text{SeCuO}_3$  obtained from torque measurements in this work. Red lines represent magnetic axes which are also extrema of the anisotropy energy. Easy axis direction (global minimum) is along  $\langle \bar{1}01 \rangle^*$  axis.

where  $\hat{\chi}$  is magnetic susceptibility tensor of the sample written in the same coordinate system as the energy (5), and  $\psi$  and  $\xi$  are polar and azimuthal angles in spherical coordinate system representing direction of magnetic field  $\mathbf{H} = H(\cos\xi\sin\psi, \sin\xi\sin\psi, \cos\psi)$ . In very low magnetic field tensor  $\hat{\chi}$  is given by (4). In finite magnetic field, spin axis will in general start to rotate from the direction of easy axis. We describe this rotation by allowing the susceptibility tensor to rotate

$$\hat{\chi}(\theta, \phi) = \mathbf{R}(\theta, \phi) \cdot \hat{\chi}_0 \cdot \mathbf{R}^T(\theta, \phi) \quad (7)$$

where  $\hat{\chi}_0$  is the low-field ( $H \ll H_{SF}$ ) susceptibility tensor given by expression (4) and  $\mathbf{R}(\theta, \phi)$  is the rotation matrix. Our torque measurements were performed at  $T = 4.2$  K where  $\chi_{[\bar{1}01]^*} = 4 \cdot 10^{-4}$  emu/mol,  $\chi_{[101]} = 3.5 \cdot 10^{-3}$  emu/mol and  $\chi_b = 3.8 \cdot 10^{-3}$  emu/mol are eigenvalues of susceptibility tensor obtained from previous susceptibility and torque measurements [6, 9].

Total phenomenological energy  $\mathcal{F}_{tot}$  of the sample in finite magnetic field is a sum of MAE and Zeeman energy

$$\mathcal{F}_{tot}(\theta, \phi, \psi, \xi) = \mathcal{F}_a(\theta, \phi) + \mathcal{F}_Z(\psi, \xi, \theta, \phi). \quad (8)$$

For anisotropic antiferromagnetic sample placed in finite magnetic field  $\mathbf{H}(\psi, \xi)$ , new direction of the spin axis is obtained numerically by minimizing the total energy  $\mathcal{F}_{tot}$  with respect to  $\theta$  and  $\phi$ . To simulate experimental results we start by finding values of anisotropy constants  $K_1$  and  $K_2$  which satisfy above mentioned requirements for MAE extrema. Correct choice of values must reproduce the experimental value of spin flop field  $H_{SF} \approx 1.8$  T at  $T = 2$  K when magnetic field is applied along easy axis. Specifically, in this case spin flop field  $H_{SF} = [2(K_1 - K_2)/(\chi_{[101]} - \chi_{[\bar{1}01]^*})]^{1/2}$  [20, 25] and by simulating dependence of magnetization on magnetic field to

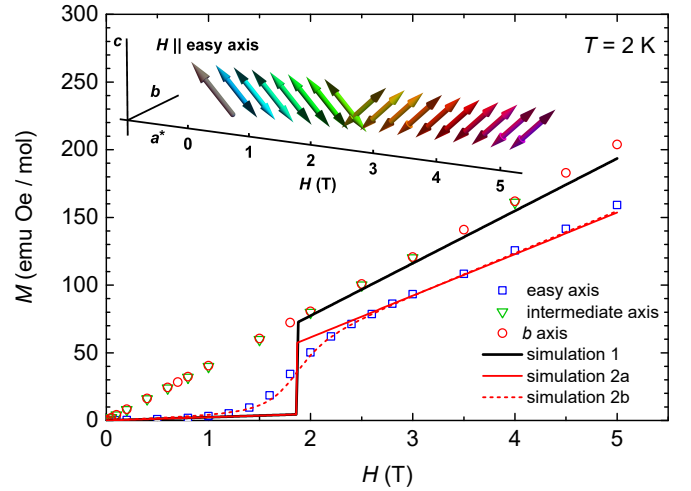


FIG. 4. Simulation of magnetization dependence on magnetic field when  $H$  is parallel to easy axis compared to experimental result at  $T = 2$  K published in Ref. 6 (empty blue squares). Inset: Spin axis direction dependence on applied magnetic field obtained from simulation. Simulation 1 allows all spins to rotate simultaneously. Simulation 2 allows only part of spins to rotate, as described in text. Solid red line (2a) represents result for  $H \parallel$  easy axis, while dashed line (2b) simulates misorientation of the sample by  $10^\circ$ , to mimic probable misorientation in experiment.

obtain the value of  $H_{SF}$  we can only pinpoint the difference  $K_1 - K_2$ . The values of  $K_1$  and  $K_2$  will be obtained from simulation of angular dependence of torque.

We proceed to simulate experimentally obtained dependence of magnetization on magnetic field for field applied along easy axis direction at  $T = 2$  K. Setting  $K_2 - K_1 = -6.35 \cdot 10^5$  erg/mol gives  $H_{SF} = 1.87$  T for values of susceptibility tensor measured at  $T = 2$  K [9]. We fix our spin flop field to this value since it is well within the margin of error for experimental data, and it also reproduces our other results well. We apply magnetic field  $\mathbf{H}(\psi_0, \xi_0)$  along easy axis by setting  $\psi_0 = \pi/2$ ,  $\xi_0 = 0$  in the chosen coordinate system and then minimize numerically total energy (8) for each value of applied field to obtain  $\theta_0$  and  $\phi_0$ . Using obtained values we calculate rotated susceptibility tensor (7) and finally magnetization from  $\mathbf{M} = \hat{\chi}(\theta_0, \phi_0) \cdot \mathbf{H}(\psi_0, \xi_0)$ . In order to simulate dc magnetization measurement we only take the component of magnetization along applied magnetic field. The result of our calculation shown by solid black line in Fig. 4 (simulation 1) is compared to measured values from Ref. 6 shown by empty blue squares in Fig. 4. Spin flop transition is clearly observed at  $H_{SF} = 1.87$  T in calculated curve.

Our simulation also gives new direction of spin axis which for  $H \geq H_{SF}$  rotate from easy axis direction to intermediate axis direction  $\langle 101 \rangle$ , as shown in inset of Fig. 4. However, for  $H > H_{SF}$  calculated magnetization (solid black line in Fig. 4) is somewhat larger than measured one (empty blue squares) and in fact falls on values obtained for magnetization measured along intermediate and hard axes (empty green triangles and red circles in Fig. 4). We should mention here that our result is what is usually obtained in experimental spin flop. Sig-

nificantly smaller magnetization observed in experiment is in fact anomalous and suggests the spin reorientation in  $\text{SeCuO}_3$  might be unconventional. We will return to this point later. Experimental value of spin flop field is the same at 4.2 K as at 2 K, within the experimental uncertainty [6]. Since susceptibility tensor components are slightly different at 4.2 K, we need to take  $K_2 - K_1 = -5.42 \cdot 10^5$  erg/mol in order to reproduce  $H_{SF} \approx 1.87$  T at  $T = 4.2$  K

Finally, we proceed with calculating angular dependence of torque for all planes probed during the measurements. We simulate rotation of magnetic field by appropriately changing  $\psi$  and  $\xi$  for  $\mathbf{H}(\psi, \xi)$ . By minimizing the total energy (8) we obtain the rotated susceptibility tensor from which we calculate magnetization  $\mathbf{M}$  expressed in emu Oe/mol, as described above. Then we calculate torque from  $\tau = m/M_{mol} \mathbf{M} \times \mathbf{H}$ , and plot only the component perpendicular to the plane of rotation of magnetic field, since only that component is measured in experiment.

Results obtained for  $ac$  plane shown by dashed lines are compared to measured torque curves in Fig. 5. For the  $ac$  plane, our simulations agree very well with measurements for  $H \leq 2$  T. However, for higher magnetic field calculated curves have smaller amplitude than measured curves, and the discrepancy increases as the field increases. In order to understand the discrepancy between calculated and measured amplitudes  $\tau_0$ , we compare measured and calculated  $H^2$  dependence of  $\tau_0$  in the  $ac$  plane in Fig. 2(b). Measured amplitude increases nonlinearly with  $H^2$  in low magnetic field, and for  $H > 2$  T the increase becomes linear in  $H^2$ , as we already pointed out in Section III A. In comparison, calculated torque amplitude follows the measured one below  $H \lesssim 2$  T and then it becomes constant for  $H \geq H_{SF}$  [empty squares in Fig. 2(b)]. Independence of torque amplitude on magnetic field for  $H \geq H_{SF}$  obtained from our calculation is also observed in torque experiment for conventional spin reorientation in uniaxial collinear antiferromagnet [25, 26] and is in agreement with the results of Néel [17, 18]. Our experimental result points to more exotic spin reorientation in  $\text{SeCuO}_3$ , so in the remainder of this section we consider possible reasons for the deviation of measured data from the results expected for conventional uniaxial collinear antiferromagnet.

Deviation of our experimental curves from the calculated ones could be a consequence of symmetry lowering. Symmetry lowering would result in MAE shape different from the one shown in Fig. 3 and consequently could influence measured angular dependencies of torque. However, symmetry lowering can be disregarded, as we explained earlier.

Another possibility for observed discrepancy is misorientation of the sample. Simulation of misorientation of the sample showed that increase in torque amplitude mimicking the measured one can be reproduced only for unrealistic assumption of misorientations of  $\approx 50^\circ$  or so, which were certainly not realized in experiment.

Having discarded symmetry lowering and misorientation as possible reasons for discrepancy of measured and simulated data, we turn again to linear increase of measured torque amplitude with  $H^2$  shown with full circles in Fig. 2(b). According to Eq. (3), we expect the amplitude to increase linearly

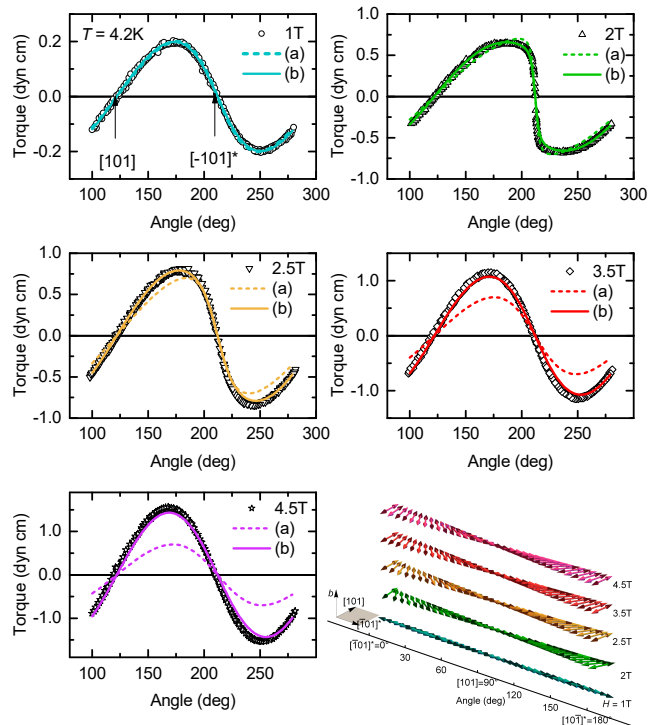


FIG. 5. Torque measured in  $ac$  plane in different magnetic fields compared to two simulations, as described in text. (a) Simulation with reorientation of all spins. (b) Simulation allowing site-specific reorientation. Bottom right panel: angle-dependent reorientation of the spin axis obtained from simulation shown in laboratory coordinate system. Plane of rotation of magnetic field is shown as dark square in accompanying coordinate system. Angle is measured with respect to  $b$  axis, while in other panels goniometer angle is shown.

with  $H^2$  when there is no spin reorientation, i.e. in antiferromagnet for  $H \ll H_{SF}$ . If all the spins in the sample would remain oriented along easy axis in applied field, torque amplitude would increase with  $H^2$  by following the dashed line in Fig. 2(b) which represents low-field behavior. Instead, for  $H \geq H_{SF}$ , data can be fitted to solid line shown in the same figure,  $\tau_0 = a + b \cdot H^2$ . Result of the fit gives  $a = (0.47 \pm 0.1)$  dyn cm and  $b = (0.0539 \pm 0.0009)$  dyn cm / T<sup>2</sup>. Using Eq. (3), we obtain from fitting constant  $b$  the following value of susceptibility anisotropy  $\Delta\chi = (8.4 \pm 0.1) \cdot 10^{-4}$  emu/mol. This value is significantly smaller than the total susceptibility anisotropy measured in the  $ac$  plane at 4.2 K in low magnetic field,  $\Delta\chi_{ac} = 3.1 \cdot 10^{-3}$  emu/mol.

The analysis given above can be interpreted as if part of the spins do not reorient in applied magnetic field, but preserve low-field behaviour described by Eq. (2). This allows us to attempt to obtain better agreement between experiment and simulation by assuming reorientation of only part of the spins. We start by dividing susceptibility tensor in two parts,

$$\hat{\chi} = \hat{\chi}_1 + \hat{\chi}_2. \quad (9)$$

In principle, one can expect different tensors  $\hat{\chi}_1$  and  $\hat{\chi}_2$  for two subsystems. However, in experiment we can only measure macroscopic total tensor  $\hat{\chi}$ . So, we try to simulate our

data by making a simple reasonable assumption: both subsystems participate in long range antiferromagnetic order, and thus their tensors are described by measured tensor (4). However, following result of Ref. [10] which claims the magnetic moments on different Cu sites are different, we allow different weight for  $\hat{\chi}_1$  and  $\hat{\chi}_2$ . Consequently, we write for tensors of separate subsystems

$$\begin{aligned}\hat{\chi}_1 &= n \hat{\chi}_0, \\ \hat{\chi}_2 &= (1-n) \hat{\chi}_0,\end{aligned}\quad (10)$$

where  $\hat{\chi}_0$  is given by Eq. (4). Expression (10) is written under assumption that both tensors share magnetic eigenaxes. Parameter  $n$  describes contribution of tensor  $\hat{\chi}_1$  to total tensor  $\hat{\chi}_0$ , i.e. contribution of induced magnetization of subsystem 1 to total magnetization  $\mathbf{M} = \mathbf{M}_1 + \mathbf{M}_2 = (\hat{\chi}_1 + \hat{\chi}_2) \cdot \mathbf{H}$ . In the following we choose  $\hat{\chi}_1$  as the susceptibility tensor of the spins that do not reorient in finite magnetic field and  $\hat{\chi}_2$  as the tensor which is allowed to rotate in applied magnetic field. Rotation of tensor  $\hat{\chi}_2$  is described by Eq. (7) where instead of  $\hat{\chi}_0$  we put  $\hat{\chi}_2$  from expression (10).

To fix the value of  $n$  we calculate again the dependence of magnetization on magnetic field and compare it to measured values in Fig. 2. Since we assume only spins of the subsystem 2 reorient,  $H_{SF} = [2(K_1 - K_2)/\Delta\chi_2]^{1/2}$ , where  $\Delta\chi_2$  represents susceptibility anisotropy only for subsystem 2 (see Eq. (10)). To reproduce  $H_{SF} = 1.87$  T at  $T = 2$  K we set  $K_2 - K_1 = -4.95 \cdot 10^5$  erg/mol and  $n = 0.22$ . Result of simulation for these parameters is shown by red solid line (simulation 2a) in Fig. 4. Spin flop transition is sharp, as expected for perfect orientation of the sample. Furthermore, calculation now reproduces measured magnetization values in all applied fields. We expect some misorientation in experiment (less than  $10^\circ$ ) which we simulated in our calculation to obtain the result shown by dashed red curve (simulation 2b) in Fig. 4. Agreement between experimental and calculated data is excellent.

We now proceed to simulate angular dependence of torque measured at  $T = 4.2$  K assuming reorientation of only part of the spins. To reproduce reproduce  $H_{SF} = 1.87$  T we set  $K_2 - K_1 = -4.23 \cdot 10^5$  erg/mol. We also set  $n = 0.22$  as obtained above and proceed calculation with susceptibility tensor (9) values measured at  $T = 4.2$  K [6, 9]. Furthermore, now it is possible to pinpoint the values of  $K_1$  and  $K_2$  to obtain best agreement with measured torque curves. Above mentioned constrictions on anisotropy constants leave two choices for sign of  $K_1$ :  $K_1 > 0$  results in easy axis kind of anisotropy, while  $K_1 < 0$  results in anisotropy shape that is closer in shape to easy plane kind of anisotropy. Our data could be well described only by assuming  $K_1 < 0$ . From our simulations we find that measured torque for all orientations is best described by following values of anisotropy constants:  $K_1 = -0.6 \cdot 10^5$  erg/mol and  $K_2 = -4.83 \cdot 10^5$  at 4.2 K. Magnetocrystalline anisotropy energy with those anisotropy constants is shown in Fig. 3. The result for  $ac$  plane is shown by solid lines in Fig. 5. Agreement with experiment is now quite remarkable. In Fig. 6 we compare torque measurements for fields rotating in the plane spanned by  $b$  and  $[\bar{1}01]^*$  axes to simulation in the plane spanned by easy and hard axis. Sharp

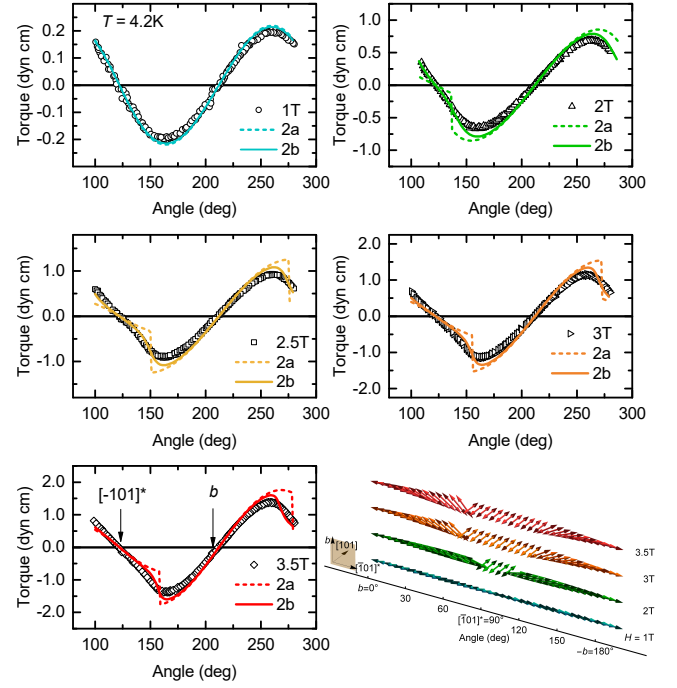


FIG. 6. Torque measured in plane spanned by axes  $b$  and  $[\bar{1}01]^*$  compared to results of simulation, as described in text. Dotted lines represent perfect orientation (2a), and solid lines are results for simulation of slightly misoriented sample (2b). Only site-specific simulation is shown. Bottom right panel: Angle-dependent spin axis reorientation for perfect orientation of the sample shown in laboratory coordinate system. Plane of rotation of magnetic field is shown as a dark square in accompanying coordinate system. Angle is measured with respect to  $b$  axis, while in other panels goniometer angle is shown.

transitions are expected for perfect orientation (dashed curves) while simulation of small misorientation (solid lines) gives better agreement with experiment. In both Fig. 5 and Fig. 6 in bottom right panel we plot simulated reorientation of spin axis corresponding to torque curves measured in different fields. Finally, in Fig. 7 we see excellent agreement between the result for the plane spanned by  $b$  and  $[101]^*$  axes and the one obtained by simulation. However, in this plane there is no reorientation in applied field for obtainable values of magnetic field, so results in this plane are not sensitive to whether we allow all spins to rotate or just part of them.

### C. Magnetic properties estimated from Density Functional Theory

In parallel to our experimental investigations of the magnetic anisotropy of  $\text{SeCuO}_3$ , we have carried out density functional theory (DFT) calculations including spin-orbit coupling (SOC), using a similar strategy to the one we considered for the low-dimensional magnetic compound  $\text{CuO}$  [27]. Indeed, we demonstrated that the estimation of the MAE of  $\text{CuO}$ , considering its antiferromagnetic ground state, allows to properly predict its easy axis of magnetization. In contrast to  $\text{CuO}$ ,

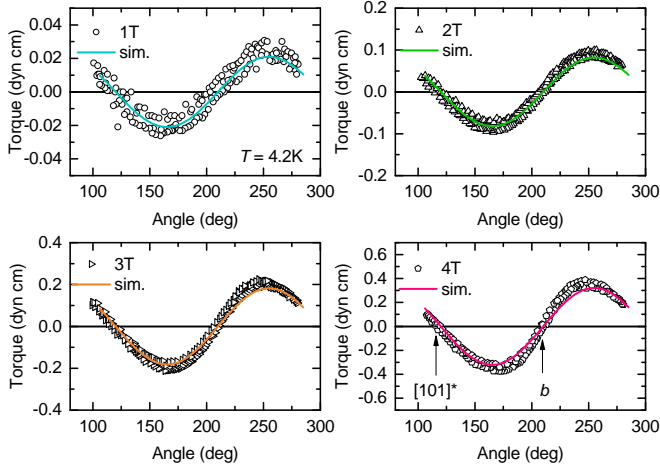


FIG. 7. Torque measured in plane spanned by axes  $b$  and  $[101]^*$  compared to results of site-specific simulation (sim.), as described in text.

spin-fluctuations seem to play a major role in  $\text{SeCuO}_3$  magnetic properties. Živković *et al.* have already pointed out the possibility to observe these quantum fluctuations in  $\text{SeCuO}_3$ , and evoked a possible difference of the magnetic moment values between Cu1 and Cu2 sites [6]. More recently, Lee *et al.* mentioned that the site-specific spin correlation may be explained by considering two subsystems based on strongly coupled Cu1 dimers and weakly interacting Cu2 spins [11]. They conclude that such a scheme will lead to smaller ordered magnetic moments for Cu1 than for Cu2 due to singlet fluctuations. Also, the reduced ordered magnetic moment of Cu1 sites has been confirmed based on neutron powder diffraction and NQR measurements [10]. However, none of the magnetic models proposed so far allows to explain all the experimental measurements. It is thus essential to provide a theoretical basis to clarify the present picture.

Our previous investigation, based on magnetic susceptibility measurements, leads to the conclusion that the Cu2-Cu1-Cu1-Cu2 tetramer is based on two antiferromagnetic couplings, namely  $J_{11} = 225$  K and  $J_{12} = 160$  K [6]. Thus, we have generated an antiferromagnetic order noted  $\text{AF}_1$  shown in Fig. 8(a) respecting these conditions, which has been used to estimate the MAE of  $\text{SeCuO}_3$  with the Wien2k code.

SOC is included as a perturbation of the antiferromagnetic collinear state, leading to an energy lowering given by

$$\Delta E_{\text{SOC}} = \frac{\left| \langle i | \hat{H}_{\text{SOC}} | j \rangle \right|^2}{|\epsilon_i - \epsilon_j|} \quad (11)$$

which accounts for an interaction between an occupied state  $i$  with an energy  $\epsilon_i$  and an unoccupied state  $j$  with an energy  $\epsilon_j$  via the matrix element  $\langle i | \hat{H}_{\text{SOC}} | j \rangle$ . The resulting MAE is represented in Fig. 9(b), showing an uniaxial anisotropy along the  $b$  direction, while hard axis is in the  $ac$  plane. A similar result is observed considering the on-site PBE0 hybrid functional. To be more quantitative, Tab. I gathered the MAE

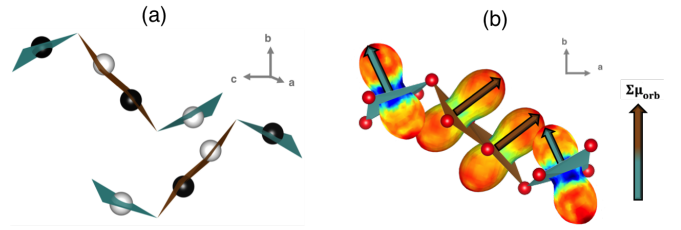


FIG. 8. (a) Antiferromagnetic order considered in our DFT calculations. The  $\text{Cu}^{2+}$  sites are depicted as filled and empty circles, representing up-spin and down-spin, respectively. (b) Orbital moment of one tetramer. Red and blue colors evidenced maximum and minimum of the orbital moment, respectively. The arrow on the right side evidences the vectorial summation of orbital moments represented by brown and blue vectors on Cu1 and Cu2 sites, respectively.

values for the magnetic eigenaxes of the AFM state (below  $T = 6$  K), deduced from torque measurements and highlighted in Fig. 3. Given values are expressed relatively to the MAE in the  $[010]$  crystal direction.

First of all, we have tested two different functionals, i.e. GGA+U and on-site PBE0 hybrid. It appears that GGA+U with  $U_{\text{eff}} = 5$  eV leads to similar MAE values to the ones obtained with PBE0. The difference between the easy axis (along  $b$ ) and the two others directions is about  $10 \mu\text{eV}/\text{f.u.}$  If we consider a larger correction ( $U_{\text{eff}} = 9$  eV) as in Ref. 28 for  $\text{SrCu}_2(\text{BO}_3)_2$ , the MAE values are reduced by a factor of two, but the trend is conserved, i.e.  $b$  is still predicted to be the easy axis in disagreement with the experimental facts. To understand this discrepancy, we first consider the Bruno relation [29]. According to this model, which is based on the SOC perturbation expression of Eq. (11) and ignoring spin-flip terms, the MAE is directly proportional to the orbital moment anisotropy

$$\text{MAE} = E_{\text{hard}} - E_{\text{easy}} = \frac{\xi}{4} \left| \langle L_z \rangle_{\text{hard}} - \langle L_z \rangle_{\text{easy}} \right| \quad (12)$$

where  $\langle L_z \rangle$  is the orbital angular momentum. The  $\langle L_z \rangle$  term in Eq. (12) is shown in Fig. 8(b) for the four copper sites of one tetramer. For clarity, arrows highlight the direction for which

TABLE I. MAE values ( $\mu\text{eV}/\text{f.u.}$ ) for the magnetic eigenaxes of the AFM state, obtained with PBE0, GGA+U with  $U_{\text{eff}} = 9$  and 5 eV (noted 9 and 5, respectively) or by substituting zinc for copper (noted Zn). Directions  $[\bar{1}01]^*$  and  $[101]$  represent easy and intermediate axes obtained from experiment.

$U_{\text{eff}}^{\text{Cu1}}/U_{\text{eff}}^{\text{Cu2}}$	$[101]$	$[\bar{1}01]^*$
9/9	4	5
9/Zn	-2	-1
Zn/9	5	9
5/5	9	9
5/Zn	-4	-2
Zn/5	11	19
PBE0/PBE0	11	14

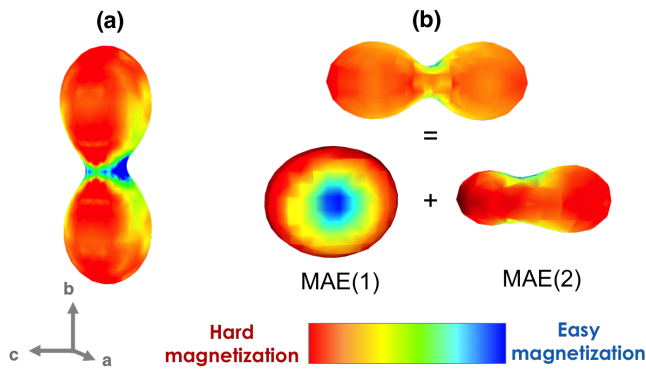


FIG. 9. (a) Experimental MAE, (b) Contributions MAE1 (MAE2) to the total MAE (top) determined substituting Cu2 (Cu1) by Zn atoms and considering an  $U_{eff} = 5$  eV correction for Cu sites.

the orbital momentum is maximum, pointing along the normal of each  $\text{CuO}_4$  plaquette. Summing the orbital moment of all copper sites leads to a total orbital moment which is maximal along the  $b$  direction, i.e. an easy magnetization axis is along  $b$ . Thus, both arguments based on orbital moments and total energy lead to the same conclusion, i.e. an easy axis along the  $b$  direction, in contradiction to the experimental data. It should be noticed that as expected for a spin-half system, the dipolar contribution is negligible, less than  $0.7 \mu\text{eV/f.u.}$

In addition, the present DFT calculations cannot reproduce another experimental fact which is the different magnetic moments at Cu1 and Cu2 sites,  $0.46$  and  $0.73 \mu_B$ , respectively, from NPD [10]. Indeed, DFT gives similar magnetic moments for Cu1 and Cu2, i.e.  $0.84$  and  $0.75 \mu_B$  considering  $U_{eff} = 9$  and  $5$  eV, respectively. While  $U_{eff} = 5$  eV allows to properly describe the magnetic moment of Cu2, it cannot explain reduced value obtained from experiment for the Cu1. Such a feature appears to be related to the fact that, as in  $\text{CdCu}_2(\text{BO}_3)_2$ , Cu1 ions form strongly coupled singlets, which are polarized by the staggered field of Cu2 spins, and Cu1 and Cu2 magnetic subnetworks are decoupled.

We have then estimated the contribution of each inequivalent copper site to the MAE. MAE of Cu1 sites (noted MAE1) was calculated by substituting zinc for copper on all Cu2 sites, and MAE of Cu2 sites (noted MAE2) reversely [30]. Indeed,  $\text{Zn}^{2+}$  and  $\text{Cu}^{2+}$  cations share nearly the same radii,  $0.74$  and  $0.71 \text{ \AA}$ , respectively. In addition,  $\text{Zn}^{2+}$  is non magnetic ( $d^{10}$  electronic configuration) allowing suppression of magnetic response of Zn-substituted sites. A representation of these partial MAE is given in Fig. 9(b). In particular, the easy magnetization axis is located in the  $ac$  plane and along the  $b$  direction for MAE1 and MAE2, respectively. However, MAE2 is larger in amplitude than MAE1, leading to a total contribution to MAE dictated by MAE2, i.e. an easy axis along the  $b$ .

Our calculations evidence the predominant role of the Cu2 subnetwork in the magnetic anisotropy of  $\text{SeCuO}_3$ , but remain incomplete because we do not reproduce the magnetic moment reduction of Cu1. As already mentioned above, such a feature is a consequence of the formation of Cu1 dimers which are in a singlet state at low temperature ( $T < 200$  K),

the spin fluctuations of Cu1 spins which are different from the ones of Cu2, leading to the decoupling of the two subnetworks, and the staggered field of Cu2 subnetwork which polarizes the magnetic moments of Cu1, leading to a strong decrease of its value [5].

From our point of view, all these experimental data converge to one model for  $\text{SeCuO}_3$ , consisting of nearly isolated Cu1 dimers immersed in the staggered field of the AFM long range order of the Cu2 subnetwork. One simple approach is to reduce the Hubbard correction on Cu1 site, and indeed this leads to decrease of Cu1 magnetic moments from  $0.84$  to  $0.75$  and  $0.60 \mu_B$ , with  $U_{eff} = 9, 5$  and  $0$  eV, respectively. Reducing  $U_{eff}$  even more to negative values will lead to entering an attractive electron-electron interaction regime. Such attractive Hubbard model has been previously used as an effective description for systems involving strong electron-phonon coupling [31]. Indeed, strong spin-lattice coupling in the low-temperature state of  $\text{SeCuO}_3$  has been evidenced by Lee *et al.*, based on the measurement of the nuclear spin-lattice relaxation rate  $1/T_1$  [11].

Here, the idea is to simulate an extreme situation for which the electron-phonon coupling involving the Cu1 dimers would be enough to overcome the electron-electron Coulomb repulsion. It will correspond to the observation of attractive and repulsive regimes on low and high energy scales, respectively [31]. Interestingly, calculating the MAE with two sizable different treatments for Cu1 and Cu2 subnetworks reproduces the experimental observation. More specifically, we have used  $U_{eff} = 0$  eV for Cu1 and  $U_{eff} = 5$  eV for Cu2. This choice allows us to reproduce in an effective manner the magnetic moment of Cu2 and the reduction of magnetic moments of Cu1. Such treatment leads to a 3D shape shown in Fig. 10(b), for which the  $b$  direction is properly found as being the hard axis and the easy axis lying in the  $ac$  plane. To be more quantitative, we compared in Tab. II the MAE values for the magnetic eigenaxes of the AFM state with respect to the MAE value along the  $b$  axis direction. It now appears that, among these three directions,  $[0 1 0]$  is systematically the hard one, and  $[1 0 1]$  the easy one. In other words, by considering that Cu1 and Cu2 subnetworks are decoupled and by taking into account the reduction of the magnetic moment of Cu1, we are able to reproduce the experimental hard magnetization axis along the  $b$  direction. The easy axis is found to be in the  $ac$  plane in agreement with experimental refinements, but still not in the  $[\bar{1}01]^*$  direction determined from experiment (see Fig. 10).

At this stage, it should be mentioned that Bousquet *et al.* [32] have demonstrated that defining explicitly the exchange-correction parameter  $J$ , in LSDA+U treatment, strongly affects the non-collinear magnetic ground state, and more specifically the spin canting and the magnetocrystalline anisotropy shape. This constitutes a really delicate issue because it implies an adjustment of the amplitude of two parameters,  $U$  and  $J$ . Our results for  $U - J = 5 - 0.5$  eV are summarized in Tab. II. It should be noticed that a similar trend of values is obtained using  $J = 1$  eV, confirming that the more important aspect is to explicitly specify the  $J$  value. Interestingly, the experimental MAE eigenaxes are properly described as

TABLE II. MAE values ( $\mu\text{eV}/\text{f.u.}$ ) for the magnetic eigenaxes of the AFM state obtained with different GGA+U treatments for copper atoms. We report values obtained for  $U_{\text{eff}} = 5$  eV and  $U - J = (5 - 0.5)\text{eV}$ . Results are given with respect to the MAE along the  $b$  axis direction.

Cu1 / Cu2	$U_{\text{eff}}$		$U - J$	
	5 / 5	0 / 5	5-0.5 / 5-0.5	0 / 5-0.5
[101]	9	-10	-7	-26
$[\bar{1}01]^*$	9	-7	-20	-32

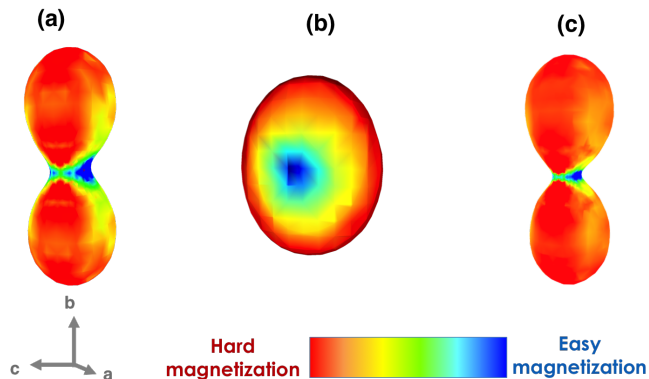


FIG. 10. (a) Experimental MAE, (b) MAE considering  $U_{\text{eff}} = 0$  eV for Cu1 and  $U_{\text{eff}} = 5$  eV for Cu2, (c) similar as previously, except a  $U - J = 5 - 0.5$  eV correction on Cu2.

soon as  $J$  is explicitly defined [see Fig. 10(c)]. More specifically, when both Cu1 and Cu2 are corrected, MAE values are 0, -7 and -20  $\mu\text{eV}\cdot\text{f.u.}^{-1}$  for the [010], [101] and  $[\bar{1}01]^*$  directions, respectively. When the correction is added only on Cu2, the MAE values are 0, -26 and -32  $\mu\text{eV}\cdot\text{f.u.}^{-1}$  for the identical respective directions. Such results evidenced a drastic change of the MAE, mainly on the intermediate eigenaxes. In such a case, both explicit  $J$  definition on Cu2 and reduced Hubbard correction on Cu1 are necessary to properly orientate the theoretical easy axis along the experimental one, as represented in Fig. 10(c). In order to verify how the MAE2 behaves with such treatment, we redo a chemical substitution by Zn atoms on Cu1 sites. As expected, the MAE is strongly modified with respect to the one determined using an  $U_{\text{eff}}$  treatment [Fig. 10(b)], i.e. with an easy, intermediate and hard axes in really good agreement with the experimental ones, as can be witnessed from Figs. 10(a) and 10(c). It should be noticed that the overall shape of the MAE was unchanged when considering  $J = 0.5$  and 1 eV for  $U = 5$  eV.

#### IV. DISCUSSION

Torque magnetometry is a convenient method for studying magnetocrystalline anisotropy and spin reorientation phenomena in finite magnetic field since angular dependence of torque is very sensitive to the orientation of spin axis. We employed this method to determine the MAE shape in antifer-

romagnetic state of  $\text{SeCuO}_3$ . Previous magnetic susceptibility results showed that, below  $T_N$ ,  $\text{SeCuO}_3$  might be considered a conventional collinear uniaxial antiferromagnet since susceptibility measured along one of the axis goes practically to zero as  $T \rightarrow 0$  (easy axis), while along other two axes  $\chi$  only slightly increases as temperature decreases [6]. This behaviour is typical for uniaxial collinear antiferromagnet [18], although it does not disqualify a very weak canting of spins. Magnetization measurement at 2 K revealed spin flop transition in field of  $H_{\text{SF}} \approx 1.8$  T applied along easy axis, also a feature of antiferromagnets with weak magnetocrystalline anisotropy [17, 18].

Using symmetry allowed MAE and experimentally determined susceptibility tensor we calculated magnetization as a function of applied field and angular dependence of torque under assumption that all spins collectively rotate in finite magnetic field. This produced results which are expected for uniaxial antiferromagnet, [18, 25, 26], but which only qualitatively agree with experiment. In  $H > H_{\text{SF}}$  the magnitude of magnetization should be equal to the value obtained when field is applied along intermediate axis, while experimental value was significantly smaller (see Fig. 4). Also, in  $H > H_{\text{SF}}$  torque amplitude is expected to become independent on applied magnetic field [25, 26], while in experiment the amplitude showed  $H^2$  dependence, but with much smaller slope than in low magnetic field. The  $H^2$  dependence of torque amplitude is characteristic for an AFM system in magnetic field  $H \ll H_{\text{SF}}$ , in which there is no reorientation of spins. This led us to perform simulations where we distinguished two separate subsystems, each represented by its own susceptibility tensor,  $\hat{\chi}_1$  and  $\hat{\chi}_2$ . Tensor of one subsystem,  $\hat{\chi}_1$ , remains fixed in applied magnetic field, while tensor of the other subsystem,  $\hat{\chi}_2$ , is allowed to rotate. In this way we obtained quantitative agreement of our simulations with both magnetization and torque experiment (see Figs. 4 - 7).

The possibility of existence of two subsystems was already mentioned in Ref. 6 where it was suggested that correlations between Cu1 and Cu2 in  $\text{SeCuO}_3$  are site-selective and strong coupling between Cu1 spins might form a singlet state at higher temperatures thus separating Cu1 from Cu2 spin sublattice. The scenario of two subsystems made of strongly coupled Cu1 dimers and weakly coupled Cu2 spins in the AFM state was recently proposed from NMR measurements which witnessed different temperature evolution of  $1/T_2$  assigned to Cu1 and Cu2 spins in AFM state [11]. NQR measurements showed that Cu1 dimers indeed form singlets already at high temperatures  $T < 200$  K, while Cu2 spins are only weakly coupled to the central pair [10].

These results allow us to construct more rigorous model of the spin reorientation in  $\text{SeCuO}_3$ . Previously published susceptibility anisotropy in the AFM state strongly supports picture of collinear or very weakly canted AFM state in zero magnetic field [6, 9]. From our macroscopic measurements we are not able to discern the canting so we proceed with collinear picture. Magnetically ordered state which complies with our torque measurements both previous [9] and from this work is shown in Fig. 11(a) and 11(c). Our theoretical investigations based on the similar magnetic ordering do not allow

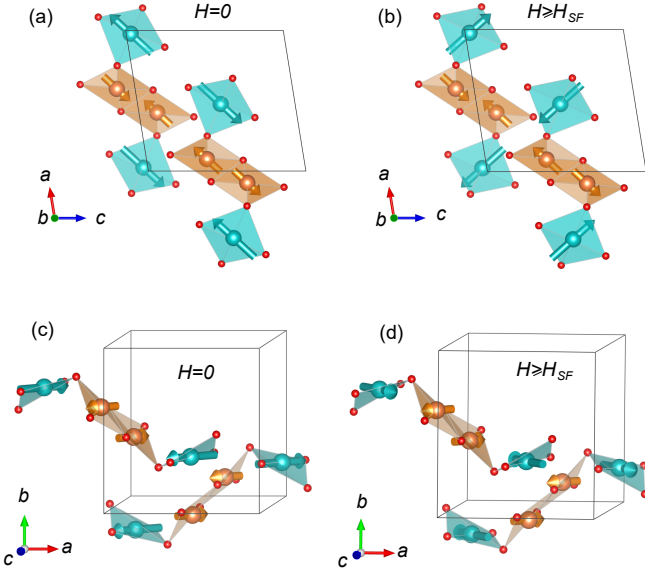


FIG. 11. Magnetic structure in AFM state in zero field (a) and (c) and if field  $H \geq H_{SF}$  applied along easy axis (b) and (d) obtained in this work. (a) and (b) show  $ac$  plane to which the spins are confined.

us to obtain a better picture of this magnetic ordering. Moreover, actual magnetic structure cannot be determined from our macroscopic experiment, only orientation of collinear spins with respect to crystal axes. To propose specific orientation of spins shown in Fig. 11(a) and 11(c), we rely on symmetry elements as well as results from literature which allow us to assume AFM coupling between Cu1 spins [10] and AFM coupling between Cu1 and Cu2 spins on tetramer [6]. In zero field all spins are oriented along  $\langle \bar{1}01 \rangle^*$  direction (Ref. [9] and this work). This result is in disagreement with neutron powder diffraction data which propose a very noncollinear magnetic structure [10]. We point out here that structure from Ref. 10 is in disagreement with measured magnetic susceptibility anisotropy [6, 9] which can only allow collinear or very weakly canted spins, as we mentioned above. Large canting proposed in Ref. 10 would not produce magnetic susceptibility measured along easy axis which goes to zero as  $T \rightarrow 0$  [6], a typical feature of collinear or only very slightly canted antiferromagnet.

In order to confirm the present picture, we have realized DFT+U+SOC calculations [13, 33] using the VASP code [34–36] to take into account the potential non-collinearity. More specifically, we have used an energy cutoff of 550 eV, a similar  $k_{\text{mesh}}$  to the one in Wien2k and the convergence criterion was fixed at  $10^{-7}$  eV. Starting from a collinear antiferromagnetic arrangement with all the spins oriented along the  $\langle \bar{1}01 \rangle^*$ , we obtained a small but significant non-collinearity between Cu1 and Cu2 spins, with a canting angle ranging from 0.2 to  $1^\circ$  depending on the  $U$  (from 5 to 7 eV) and  $J$  (from 0 to 1 eV) values. This last result confirms that  $\text{SeCuO}_3$  can be viewed as a slightly canted antiferromagnet, but the canting is too weak to produce an effect in our macroscopic measurements. It also justifies the Wien2k calculations reported in the present paper, which have been done using a collinear

antiferromagnetic model. These calculations have evidenced that an explicit definition of the exchange-correction term  $J$  in the GGA+U+SOC calculations is needed to properly describe the MAE eigenaxes. Moreover, by taking into account, in an effective manner, the different correlation regime of Cu1 and Cu2 subnetworks, we are able to reproduce the reduction of the Cu1 magnetic moment and the relative amplitudes of MAE1 and MAE2.

A chemical interpretation of these results can be reached by examining the projected densities of states (pDOS). Indeed, such analysis allows to determine the most important interactions, which are the ones with the smallest energy gap  $|\epsilon_i - \epsilon_j|$ , as defined in Eq. (11). More precisely, the observed spin orientations of such  $\text{Cu}^{2+}$   $S = 1/2$  system can be interpreted by the inspection of the pDOS and thus the interactions involving the crystal-field split  $d$ -states of each magnetic  $\text{Cu}^{2+}$  ion, under the action of the spin-orbit coupling. Figs. 12(a) and 12(b) show the split of Cu1 and Cu2  $d$ -states using GGA+U calculations, with  $U_{\text{eff}} = 5$  eV. It should be noted that the pDOS obtained with and without specifying explicitly the exchange-correction term  $J$  are similar. Here, we defined the local coordinate system with  $x$  and  $y$  inside the  $\text{CuO}_4$  plane, pointing towards oxygen atoms, and  $z$  perpendicular to the  $\text{CuO}_4$  plaquette as shown in Fig. 12(a). The overall features for pDOS of Cu1 and Cu2 are the same, with an empty  $(x^2 - y^2)$  state. In such a situation, the  $\langle d_{xy} \downarrow | \hat{H}_{\text{SOC}} | d_{x^2-y^2} \downarrow \rangle$ ,  $\langle d_{xz} \downarrow | \hat{H}_{\text{SOC}} | d_{x^2-y^2} \downarrow \rangle$  and  $\langle d_{yz} \downarrow | \hat{H}_{\text{SOC}} | d_{x^2-y^2} \downarrow \rangle$  interactions will be non-zero and mainly active because closer to the Fermi level. Spins with orientation inside the plaquette ( $\parallel xy$  spin orientation) will be favored if  $d_{xz} \downarrow$  or  $d_{yz} \downarrow$  states are closer to the empty  $d_{x^2-y^2} \downarrow$  states. In contrast, if  $d_{xy} \downarrow$  states are closer, spins with orientation perpendicular to the  $\text{CuO}_4$  plaquette ( $\perp xy$  spin orientation) will be favored. In the present case, the interpretation is not straightforward due to the significant distortion of Cu1 and Cu2 sites, which are far from regular  $\text{CuO}_4$  plaquettes. Only Cu1 pDOS show relevant features, which can be interpreted. Indeed, the inset of Fig. 12(b) shows that the states which are mainly contributing on the top of the valence band are  $d_{xz}$  and  $d_{yz}$ , which leads to favour the  $\parallel xy$  spin orientation, as evidenced in our DFT+U+SOC calculations when considering only Cu1 subnetwork, i.e. MAE1 which shows an easy magnetization axis in the  $ac$  plane. In contrast, Cu2 pDOS does allow us to evidence which  $d$ -state is mainly contributing to the top of the valence band. Indeed, while such an analysis is relevant for systems exhibiting regular environments, it should be used with care for distorted environments, because the choice of the local axes for the pDOS is not anymore unique and may influence the results. Fig. 12(c) shows the pDOS of Cu1 when considering no Hubbard correction ( $U_{\text{eff}} = 0$  eV). The main consequence is a significant band gap reduction and an increase of the  $d_{xz}$  and  $d_{yz}$  characters on the top of the valence band. Both modifications lead to an increase of the spin-orbit coupling which mixes the  $d_{xz}$  and  $d_{yz}$  occupied states with the  $d_{x^2-y^2}$  unoccupied state. Such treatment leads to have a larger contribution of MAE1 to the total MAE, which then develops an easy axis in the  $ac$  plane and

hard axis along the  $b$  crystallographic direction.

To summarize, there are some similarities between structure from Ref. 10 and our proposal shown in Fig. 11(a) and 11(c). Magnetic moments on Cu2 are almost in the CuO<sub>4</sub> plaquette in both cases and general direction seems to be similar although it is difficult to make quantitative comparison since authors in Ref. 10 only plotted magnetic structure and did not explicitly provide directions of the magnetic moments. Moments on Cu1 in our structure are neither inside the plaquette nor perpendicular to it, similar to what is proposed by neutron diffraction [10]. The direction of moments on Cu1, however, is in our case very different from the one given in Ref. 10. Our results state that Cu1 moments should be collinear or almost collinear to Cu2 moments, in agreement with susceptibility, magnetization and torque data, while neutron powder diffraction gives a very noncollinear structure [10]. Further investigation of magnetic structure by neutron diffraction on single crystal would resolve this issue.

Torque data presented in this work suggest reorientation for only part of the spins in SeCuO<sub>3</sub> in magnetic field comparable to the spin flop field. Present DFT calculations and results from literature [10, 11] allow us to propose that this partial reorientation is in fact site-specific reorientation. Since NMR measurements witness two separate subsystems in AFM state [11], while NQR shows existence of strongly coupled singlet [10], we propose that susceptibility tensor which rotates in finite magnetic field corresponds to Cu2 spins, while Cu1 spins do not reorient in field applied in our experiment. This results in magnetic structure shown in Fig. 11(b) and 11(d) for  $H \geq H_{SF}$  applied along easy axis, where spins on Cu2 rotate in the  $ac$  plane and are perpendicular to spins on Cu1. This supports the picture where Cu1 and Cu2 subsystems are decoupled in some way. Since half of spins in SeCuO<sub>3</sub> are Cu1 spins, and another half Cu2 spins, we can now write for susceptibility of Cu1 given in Eq. (10)  $\chi_1 = n\chi_0 = m \cdot (0.5 \cdot \chi_0)$ . In this equation,  $0.5 \cdot \chi_0$  presents the total contribution the Cu1 spins would give to susceptibility if they were equivalent to Cu2 spins, and in our model this contribution is reduced by  $m$  due to decoupling of Cu1 and Cu2 sublattices. For obtained value  $n = 0.22$  we get  $m = 0.44$ . Magnetization induced by magnetic field on Cu1 spins is only 44% of the value it would have if these spins were equivalent to Cu2 spins. It is tempting to compare this to the ratio of magnetic moments  $m_{Cu1}/m_{Cu2} \approx 0.4/0.7 = 0.57$  obtained for magnetic moments on Cu1 and Cu2 from neutron data [10]. However, this comparison may not be justified if Cu1 and Cu2 belong to decoupled subsystems. The ratio  $\chi_1/\chi_2 = n/(1-n) = 0.282$  confirms that magnetization induced on Cu2 spins is significantly larger than on Cu1 spins. This picture corroborates more important contribution of the Cu2 site in the total MAE.

The separation of Cu1 and Cu2 subsystems is comparable to what is observed in Cu<sub>2</sub>Cd(BO<sub>3</sub>)<sub>2</sub> [3]. The question in SeCuO<sub>3</sub> is, are the Cu1 spins polarized singlets in the underlying AFM state formed by interaction between Cu2 spins, or do both Cu1 and Cu2 spins interact mutually to form the AFM state? If Cu1 spins indeed form singlet states even in AFM state, their susceptibility and susceptibility anisotropy should be much smaller than that of antiferromagnetically or-

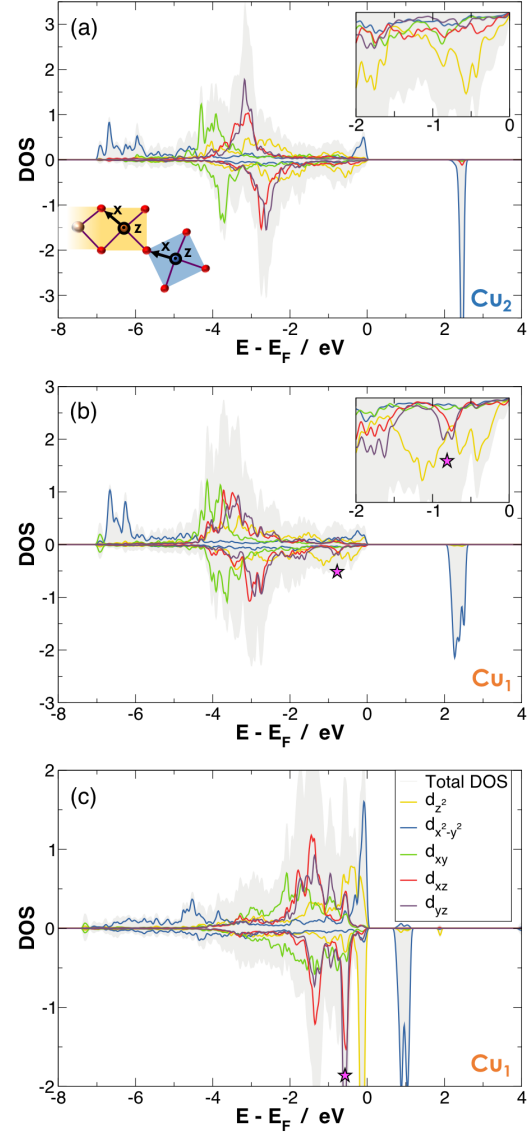


FIG. 12. Projected density of states (pDOS) on (a) Cu2 and (b) Cu1 sites considering an  $U_{eff} = 5$  eV, and on (c) Cu1 only at the GGA level. Projection axes for each Cu site is represented on the scheme in (a). Insets zoom the spin minority states over the range of 2 eV below the Fermi energy. Pink stars evidence first excitations allowed with the excited states.

dered Cu2 spins. In fact, if true singlet state persists in AFM state, for intradimer interaction  $J \approx 200$  K between Cu1 spins we should expect susceptibility and its anisotropy to be zero at low temperatures [37]. Finite slope of torque amplitude for non-flopped spins [see Fig. 2] suggests Cu1 spins contribute with finite susceptibility anisotropy. Also,  $\chi_1/\chi_2 = 0.282$  obtained from our simulations is small but finite. From our data we cannot distinguish if Cu1 spins in AFM state form polarized singlets or contribute to AFM order with much smaller magnetic moment than Cu2 spins. Site-specific spin reorientation we observe favors the former picture, but further experiments are needed to confirm this.

If Cu1 spins are in fact polarized singlets, neutron diffraction result for Cu2 sublattice [10] would then be in agreement with other experimental data as well. For  $\text{CdCu}_2(\text{BO}_3)_2$  neutron diffraction gave sizable magnetic moment on Cu1 sites [4], while theoretical and experimental data showed that Cu1-Cu1 dimer in fact forms singlet in AFM state [3, 5]. A similar scenario appears to apply to  $\text{SeCuO}_3$ , and indeed our DFT calculations, mimicking the reduction of the magnetic moment of Cu1 site, reproduce properly the experimental MAE. Magnetic order in  $\text{CdCu}_2(\text{BO}_3)_2$  is almost collinear with very small canting, similar to what we propose for  $\text{SeCuO}_3$ . One way to check our proposed magnetic structure in zero and finite field rigorously is to perform single crystal neutron diffraction experiment in zero and applied magnetic field.

## V. CONCLUSION

The present paper proposes a combined experimental and theoretical investigation of the magnetic properties of a low-dimensional spin 1/2 system, which appears to be based on two decoupled magnetic subsystems. This finding, based on measurements on high-quality single crystals and state of the art density functional calculations, is opening the way to very exciting physics, with the possibility to control separately two magnetic subsystems in one material.  $\text{SeCuO}_3$  was previously proposed as a candidate for a system with site-selective spin correlations where Cu1 copper atoms form strongly coupled AFM dimers, while coupling including Cu2 spins results in long range AFM order at low temperatures. Our torque magnetometry results evidence site-specific spin reorientation in applied magnetic field in AFM state of  $\text{SeCuO}_3$ . Using ab-initio approach we show that Cu1 and Cu2 contribute differently to the magnetic anisotropy energy. These results strongly suggest that Cu1 and Cu2 spin systems are decoupled in  $\text{SeCuO}_3$ . Combining our experimental and theoretical findings we propose antiferromagnetic structure of  $\text{SeCuO}_3$  in zero field, as well as in field  $H \gtrsim H_{SF}$ , to be challenged by future experiments on this system.

## ACKNOWLEDGMENTS

M. H., N. N., Ž. R. and M. D. acknowledge full support of their work (torque experiment and simulation of torque data) by the Croatian Science Foundation under Grant No. UIP-2014-09-9775. M. H., M. D., W. L.-d.-H. and X. R. acknowledge support by COGITO project "Theoretical and experimental investigations of magnetic and multiferroic materials" funded by Croatian Ministry of Science and Education and The French Agency for the promotion of higher education, international student services, and international mobility. W. L.-d.-H. and X. R. thank the CCIPL (Centre de Calcul Intensif des Pays de la Loire) for computing facilities. The theoretical work was also performed using HPC resources from GENCI-[TGCC/CINES/IDRIS] (Grant 2017-A0010907682). Crystal and magnetic structures in this work were drawn using 3D visualization program VESTA [38].

## Appendix: Torque magnetometry, susceptibility tensor and magnetic axes

For sample with magnetization  $\mathbf{M}$  placed in magnetic field  $\mathbf{H}$  magnetic torque  $\boldsymbol{\tau}$  acting on the sample can be written as

$$\boldsymbol{\tau} = V \mathbf{M} \times \mathbf{H}, \quad (\text{A.1})$$

where  $V$  is the volume of the sample. For systems in which response of magnetization to magnetic field is linear (such as paramagnets and antiferromagnets in magnetic field well below spin-flop field  $H_{SF}$ )  $\mathbf{M} = \hat{\boldsymbol{\chi}} \cdot \mathbf{H}$ , where  $\hat{\boldsymbol{\chi}}$  is magnetic susceptibility tensor. Taking into account Neumann's principle and symmetry restrictions for  $\text{SeCuO}_3$  [24], tensor  $\hat{\boldsymbol{\chi}}$  written in crystal axes coordinate system  $(a^*, b, c)$  is given by

$$\hat{\boldsymbol{\chi}} = \begin{bmatrix} \chi_{a^*a^*} & 0 & \chi_{a^*c} \\ 0 & \chi_{bb} & 0 \\ \chi_{a^*c} & 0 & \chi_{cc} \end{bmatrix}. \quad (\text{A.2})$$

Expression (A.2) states that  $b$  axis is one of the eigenaxes of the susceptibility tensor, or magnetic axes, while two other magnetic axes restricted to the  $ac$  plane are not necessarily along any of the the crystal axes ( $\chi_{a^*c} \neq 0$ ).

Previously published torque magnetometry results showed that in paramagnetic state, apart from axis  $b$ , eigenaxes of the susceptibility tensor in the  $ac$  plane are not in the direction of crystal axes [9]. Furthermore, torque results showed that magnetic axes in the  $ac$  plane rotate as temperature changes [6, 9]. To understand how rotation of magnetic axes can be observed in torque measurements, we write tensor  $\hat{\boldsymbol{\chi}}$  for the most general orientation of the sample in laboratory coordinate system  $(x, y, z)$

$$\hat{\boldsymbol{\chi}} = \begin{bmatrix} \chi_{xx} & \chi_{xy} & \chi_{xz} \\ \chi_{xy} & \chi_{yy} & \chi_{yz} \\ \chi_{xz} & \chi_{yz} & \chi_{zz} \end{bmatrix}. \quad (\text{A.3})$$

In experiment magnetic field is rotated in the  $xy$  plane,  $\mathbf{H} = H(\cos\phi \sin\phi, 0)$ , and only component of torque along the  $z$  axis is measured. When tensor  $\boldsymbol{\chi}$  from Eq. (A.3) is introduced in expression (A.1) we obtain for the measured component of torque  $\tau_z$

$$\tau_z = \frac{m}{2M_{mol}} H^2 [(\chi_{xx} - \chi_{yy}) \sin 2\phi - 2\chi_{xy} \cos 2\phi]. \quad (\text{A.4})$$

where  $m$  is mass of the sample given in units of  $g$ ,  $M_{mol}$  is molar mass given in  $g/mol$  and components of tensor (A.3) are expressed in  $emu/mol$ , as in experiment. Measured torque is then given in  $dyn\ cm$ .  $\phi$  is goniometer angle which describes the direction of magnetic field with respect to laboratory axes. When eigenvectors of the susceptibility tensor are along the  $x$  and  $y$  axis, the off diagonal component  $\chi_{xy}$  is zero and  $\chi_{xx}$  and  $\chi_{yy}$  represent maximal and minimal components of  $\boldsymbol{\chi}$  in that plane. Otherwise, maximal and minimal components in the  $xy$  plane will be rotated by some angle  $\theta_0$  with respect to  $(x, y)$  axis. If we term these new directions  $(x', y')$  we can write for the measured torque

$$\tau_z = \frac{m}{2M_{mol}} H^2 (\chi_{x'} - \chi_{y'}) \sin(2\phi - 2\phi_0), \quad (\text{A.5})$$

where correspondence of (A.4) and (A.5) is established through

$$\tan(2\varphi_0) = \frac{2\chi_{xy}}{\chi_{xx} - \chi_{yy}}, \quad (\text{A.6a})$$

$$\chi_{x'} - \chi_{y'} = \frac{\chi_{xx} - \chi_{yy}}{\cos(2\varphi_0)} = \frac{2\chi_{xy}}{\sin(2\varphi_0)}. \quad (\text{A.6b})$$

$\varphi_0$  is the angle that the  $x'$  axis makes with the  $x$  axis. In experiment the measured component of torque (for paramagnet and AFM in  $H \ll H_{SF}$ ) can be described by Eq. (A.5). From the amplitude of torque we obtain the susceptibility anisotropy in the plane of measurement  $xy$  defined as  $\Delta\chi_{xy} = \chi_{x'} - \chi_{y'}$ . Using equations (A.6a) and (A.6b) we can determine the difference of the diagonal tensor components  $\chi_{xx} - \chi_{yy}$ , and the off-diagonal tensor component  $\chi_{xy}$ . This approach shows that torque magnetometry, in combination with magnetic susceptibility measurement along one of directions  $x$ ,  $y$  or  $z$ , allows for determination of temperature dependence of susceptibility tensor  $\hat{\chi}$ . By diagonalizing the tensor one can then obtain temperature dependence of magnetic susceptibility along magnetic eigenaxes (or magnetic axes for short) and also the orientation of the eigenaxes with respect to crystal axes.

Determining magnetic eigenaxes is crucial in systems

where they rotate as temperature changes, as was observed in  $\text{SeCuO}_3$  in both paramagnetic and AFM state [6, 9], since magnetic eigenaxes also define the MAE shape. Namely, Neumann's principle dictates that extrema of the MAE are expected to coincide with magnetic eigenaxes. Our previous results showed that in AFM state magnetic axes rotate in  $ac$  plane. Another important result of Eq. (A.4) and Eq. (A.5) is that torque measurements can be utilized to observe symmetry lowering. In case of  $\text{SeCuO}_3$  this would mean appearance of finite tensor components  $\chi_{a^*b}$  or  $\chi_{bc}$  in tensor (A.2). In experiment this means the following. When torque is measured in any plane which contains the  $b$  axis, one of the axes  $x'$  or  $y'$  must correspond to  $b$  axis, i.e.  $\chi_{x'}$  or  $\chi_{y'}$  must correspond to  $\chi_b$ , while  $\varphi_0$  or  $\varphi_0 \pm 90^\circ$  must correspond to goniometer angle for which magnetic field is parallel to  $b$ . Lowering of symmetry can then be observed as temperature change of measured angle  $\varphi_0$  in plane containing the  $b$  axis. For purposes of this work we checked if there is symmetry breaking rotation in AFM state in planes containing  $b$  axis. Our results (not shown here) showed that, within experimental error induced by small misorientation of the sample, there is no symmetry breaking rotation on the AFM state, in agreement with recent NQR and neutron diffraction data [10]. At 4.2 K deep in AFM ordered state, our previous results [9] and our new measurements presented here show that magnetic eigenaxes are ( $[\bar{1}01]^*$ ,  $[101]$ ,  $[010]$ ).

- 
- [1] J. T. Haraldsen, T. Barnes, and J. L. Musfeldt, *Phys. Rev. B* **71**, 064403 (2005).
- [2] M. Hase, M. Kohno, H. Kitazawa, O. Suzuki, K. Ozawa, G. Kido, M. Imai, and X. Hu, *Phys. Rev. B* **72**, 172412 (2005).
- [3] W.-J. Lee, S.-H. Do, S. Yoon, Z. H. Jang, B. J. Suh, J. H. Lee, A. P. Reyes, P. L. Kuhns, H. Luetkens, and K.-Y. Choi, *Phys. Rev. B* **90**, 214416 (2014).
- [4] M. Hase, A. Dönni, V. Y. Pomjakushin, L. Keller, F. Gozzo, A. Cervellino, and M. Kohno, *Phys. Rev. B* **80**, 104405 (2009).
- [5] O. Janson, I. Rousochatzakis, A. A. Tsirlin, J. Richter, Y. Skourski, and H. Rosner, *Phys. Rev. B* **85**, 064404 (2012).
- [6] I. Živković, D. M. Djokić, M. Herak, D. Pajić, K. Prša, P. Pattison, D. Dominko, Z. Micković, D. Činčić, L. Forró, H. Berger, and H. M. Rønnow, *Phys. Rev. B* **86**, 054405 (2012).
- [7] H. Effenberger, *Z. Kristallogr.* **175**, 61 (1986).
- [8] E. Shuji, T. Tadashi, and M. Yoneichiro, *Bulletin of the Chemical Society of Japan* **48**, 1649 (1975).
- [9] M. Herak, A. Grubišić Čabo, D. Žilić, B. Rakvin, K. Salamon, O. Milat, and H. Berger, *Phys. Rev. B* **89**, 184411 (2014).
- [10] T. Cvitančić, V. Šurija, K. Prša, O. Zaharko, P. Babkevich, M. Frontzek, M. Požek, H. Berger, A. Magrez, H. M. Rønnow, M. S. Grbić, and I. Živković, ArXiv e-prints (2018), [arXiv:1801.01431 \[cond-mat.str-el\]](https://arxiv.org/abs/1801.01431).
- [11] S. Lee, W.-J. Lee, J. van Tol, P. L. Kuhns, A. P. Reyes, H. Berger, and K.-Y. Choi, *Phys. Rev. B* **95**, 054405 (2017).
- [12] P. Blaha, K. Schwarz, G. Madsen, D. Kvasnicka, and J. Luitz, TU Wien, Vienna (2001).
- [13] J. P. Perdew, K. Burke, and M. Ernzerhof, *Physical Review Letters* **77**, 3865 (1996).
- [14] V. I. Anisimov, I. V. Solov'yev, M. A. Korotin, M. T. Czyzyk, and G. A. Sawatzky, *Phys. Rev. B* **48**, 16929 (1993).
- [15] F. Tran, P. Blaha, K. Schwarz, and P. Novák, *Physical Review B* **74**, 155108 (2006).
- [16] H. J. Monkhorst, *Physical Review B* **13**, 5188 (1976).
- [17] L. Néel, *Ann. Phys.* **11**, 232 (1936).
- [18] L. Néel, *Proceedings of the Physical Society. Section A* **65**, 869 (1952).
- [19] H. Rohrer and H. Thomas, *Journal of Applied Physics* **40**, 1025 (1969).
- [20] A. N. Bogdanov, A. V. Zhuravlev, and U. K. Rößler, *Phys. Rev. B* **75**, 094425 (2007).
- [21] M. Herak, D. Žilić, D. Matković Čalogović, and H. Berger, *Phys. Rev. B* **91**, 174436 (2015).
- [22] M. Herak, M. Miljak, G. Dhalenne, and A. Revcolevschi, *Journal of Physics: Condensed Matter* **22**, 026006 (2010).
- [23] M. Herak, *Solid State Communications* **151**, 1588 (2011).
- [24] R. E. Newnham, *Properties of Materials (Anisotropy, Symmetry, Structure)* (Oxford University Press, New York, USA, 2005).
- [25] H. Uozaki, T. Sasaki, S. Endo, and N. Toyota, *Journal of the Physical Society of Japan* **69**, 2759 (2000).
- [26] M. Tokumoto, H. Tanaka, T. Otsuka, H. Kobayashi, and A. Kobayashi, *Polyhedron* **24**, 2793 (2005), proceedings of the 9th International Conference on Molecule-based Magnets (ICMM 2004).
- [27] X. Rocquefelte, K. Schwarz, P. Blaha, S. Kumar, and J. van den Brink, *Nat Commun* **4**, 2511 (2013).
- [28] G. Radtke, A. Sal, H. A. Dabkowska, M. B. Salamon, and M. Jaime, *Proceedings of the National Academy of Sciences* **112**, 1971 (2015).
- [29] P. Bruno, *Phys. Rev. B* **39**, 865 (1989).

- [30] C. Weingart, N. Spaldin, and E. Bousquet, *Phys. Rev. B* **86**, 094413 (2012).
- [31] R. Žitko, Ž. Osolin, and P. Jeglič, *Physical Review B* **91**, 155111 (2015).
- [32] E. Bousquet and N. Spaldin, *Phys. Rev. B* **82**, 220402 (2010).
- [33] A. I. Liechtenstein, V. I. Anisimov, and J. Zaanen, *Phys. Rev. B* **52**, R5467 (1995).
- [34] G. Kresse and J. Furthmüller, *Phys. Rev. B* **54**, 11169 (1996).
- [35] G. Kresse and J. Furthmüller, *Computational Materials Science* **6**, 15 (1996).
- [36] G. Kresse and D. Joubert, *Phys. Rev. B* **59**, 1758 (1999).
- [37] B. Bleaney and K. D. Bowers, *Proceedings of the Royal Society of London A: Mathematical, Physical and Engineering Sciences* **214**, 451 (1952).
- [38] K. Momma and F. Izumi, *Journal of Applied Crystallography* **44**, 1272 (2011).